Hybrid Vapor Chamber-based Cooling System for Power Electronics

George Damoulakis
Mechanical and Industrial Engineering
University of Illinois at Chicago
Chicago, IL, USA
gdamou2@uic.edu

Congbo Bao
Electrical and Computer Engineering
University of Illinois at Chicago
Chicago, IL, USA
cbao5@uic.edu

Mohamad Jafari Gukeh
Mechanical and Industrial Engineering
University of Illinois at Chicago
Chicago, IL, USA
mjafar5@uic.edu

Arani Mukhopadhyay
Mechanical and Industrial Engineering
University of Illinois at Chicago
Chicago, IL, USA
amukho4@uic.edu

Sudip K. Mazumder
Electrical and Computer Engineering
University of Illinois at Chicago
Chicago, IL, USA
mazumder@uic.edu

Constantine M. Megaridis
Mechanical and Industrial Engineering
University of Illinois at Chicago
Chicago, IL, USA
cmm@uic.edu

***Abstract* — A hybrid vapor chamber (wick-lined evaporator and wickless condenser) is fabricated and tested on a custom-made power electronic setup to demonstrate its efficacy in cooling power-semiconductor devices. The cooling method omits some metal-wick structures from the interior of the vapor chamber and replaces them with wickless, surface-energy patterned planar components. The heat sources of the tested setup are two N-Channel Metal-Oxide-Semiconductor Field-Effect Transistors (MOSFETs) of TO-247-3 packaging, which are connected in parallel to achieve higher current capability. These MOSFETs are dated Si-based semiconductor devices with very high conduction resistance, with the purpose to emulate high-power applications on a low-power experimental setup with reduced cost. Furthermore, the two semiconductor devices are switched at high frequency to emulate the modern power electronics' accelerating switching-frequency trend. The experimental setup exemplifies modern power electronics applications; therefore, it can be scaled to other power electronic systems requiring advanced cooling.**

The thermal-management technique takes advantage of the phase-changing properties of water inside a closed chamber consisting of two opposing flat plates, one serving as an evaporator and the other as a condenser. The condenser's wettability pattern increases the condensation heat transfer coefficient and provides the best method to return liquid to the evaporator. The evaporator plate is a wick-lined surface, with a 500 μm thick copper porous wick that allows the returned condensate to evaporate from the area over the two MOSFETs where heat input -and thus evaporation- is greatest.

The current vapor chamber advances our prior work on wickless and wettability-patterned platforms, and it is applied in a power-electronics system, with the potential to improve cooling performance. It demonstrates the adaptability of the design philosophy, which can be tailored to meet special thermal-management demands. The present experimental configuration represents a real-world power electronic implementation and demonstrates the hybrid vapor chamber's potential for specialized cooling applications.

Keywords — Vapor Chamber, Wickless, Wettability Pattern, Power Electronics, Switching Frequency, MOSFET, Thermal Management, Heat Transfer, Cooling

I. INTRODUCTION

With the development of novel material, fabrication, and packaging technologies [1], wide bandgap semiconductor (WBG) devices (i.e., SiC, GaN, etc.) can be easily switched at 100 kHz or more even under hard switching [2]–[4]. With the trend of increased switching frequency, the size of modern power electronic systems can be significantly reduced, and thus achieve higher power densities. However, with increasing switching frequency, WBG devices can be damaged if the heat generated from periodic switching is not properly dissipated. Liquid cooling is a widely used and effective method for thermal cooling and control. However, this method has drawbacks, such as larger sizes, weight, additional cost and operational complexity. As a result, one of the major impediments to producing next-generation high-power electronic packages with power densities more than 10^7 W/m^2 has been the reduction of junction temperatures without the use of liquid cooling [5]. The use of air over liquid cooling has several practical advantages. To start with, there is no extra complexity to the system, there is no moving liquid, pumps, pipes or chiller systems, resulting in a solution that is less expensive and more lightweight, and with no danger of catastrophic accidental cooling-liquid leaks. However, this method has the sole –but substantial- drawback of restricted cooling performance. In contrast to air convection-based cooling, phase-change heat transfer can minimize the thermal resistance of the system, such that it can fulfill safe operating criteria and improve the overall cooling performance. Therefore, passive phase-change components, such as Vapor Chambers (VC), are being utilized to improve the heat transfer performance of the system and enable efficient and safe operation of the switching semiconductors. Ju et al. [6] demonstrated a prototype planar VC with distinct hybrid-wick structures on the evaporator, an envelope casing with the coefficient of thermal expansion suited to match laser diodes. This chamber had evaporator thermal resistance of about 0.075 K/(W/cm^2) while extracting more than 1500 W from a 4 cm^2 heating region. Chen et al. [7] presented a

VC designed to cool down insulated-gate bipolar transistors for the automotive industry. The system had a copper-foam wick structure directly bonded to the power module. The VC offered a 34.6% improvement in junction temperature and a 41.6% lower total thermal resistance over traditional cooling solutions. Yi et al. [8] presented a VC with copper-foam wick interior that utilized micro-jet impingement on the condenser side, and it was specially designed for thermal management of high-power electronics. The best performing VC of this study had a minimum thermal resistance of ~0.1 K/W.

All systems mentioned above utilize different kinds of wick structures in their interior. Recent advantages of surface engineering allowed the creation of partial or entire wick-free VCs. Surface-wettability patterning does not impose capillary restrictions (i.e. significant pressure drop caused by metal wicks) and therefore can replace metal wicks in vapor chambers. A hybrid VC with a wick-lined evaporator and a wickless wettability-patterned condenser was showcased in Ref. [9]. By incorporating surface-wettability patterning inside vapor chambers, combining the fast condensate transport and the added benefit of domain-regulated dropwise and filmwise condensation, we have enhanced overall condensation performance. The aforementioned VC offers the added benefit of operating as a thermal diode (TD) [10] because it can transfer heat very efficiently in one direction but prevent it from flowing in the opposite direction. A similar design was implemented to transport heat from point to point (1-D spreading) instead of spreading it in a greater area (2-D spreading) by creating a low-profile flat heat pipe [11] with an effective thermal conductivity of 4.1 kW/(m·K). Moreover, a wick-free VC chamber featuring only wickless wettability-patterned components [12] was showcased. This apparatus was comprised entirely of wick-free elements that transport liquid by way of wetting forces generated by precise surface-wettability patterning. The condenser and evaporator plate of that system featured different geometric wettability patterns, each especially designed/engineered to transform a flat rectangular copper plate to a functional component of a low-profile VC. Lastly, following this same premise, a VC-TD apparatus consisting entirely of laser-functionalized elements was presented in Ref. [13]. This system was the first thermal-management component where structures from a femtosecond laser surface processing were utilized.

The present study introduces a hybrid VC with rectangular shape, which is fabricated and tested on a custom-made power electronic (PE) setup to demonstrate efficacy in cooling power-semiconductor devices. This VC-based cooling method employs the well-established technique of partially removing metal-wick structures from the interior of the VC and replacing them with wickless and surface-energy patterned planar components. The key difference is that the system's size, the evaporator's wick and the wettability-patterning of the condenser are unique and built particularly to address the spatially specific cooling needs of two electronic components that are generating intense heat simultaneously. The notion of hybrid VCs with wickless and wettability-patterned components is being expanded here in a real-life application exemplifying modern PE applications; therefore, the present approach can be scaled to other PE systems requiring advanced or specialized cooling.

II. MATERIALS AND METHODS

A. Fabrication Procedure

The hybrid VC fabrication procedure has been presented in our earlier work and a detailed description can be found in [9], [10]. A short summary of the procedure follows:

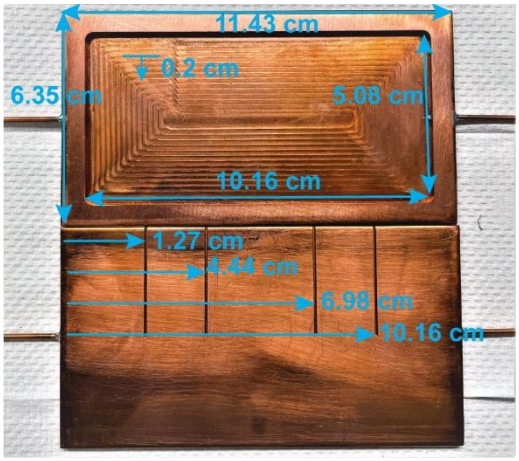

Figure 1 Photographs of an evaporator for the hybrid VC. At top, one side of the component is presented with a 2mm-deep pocket for housing the wick. The 0.2cm-wide striations mark the tracks of the milling tool used to machine the pocket. At bottom, the opposite side of the same component is showcased, where the thermocouple grooves (shown vetically) were milled. Physical dimensions for both sides are presented in cm.

1) Evaporator

Figure 1 presents photographs of an evaporator plate of the hybrid VC. Fig. 1-top shows the side of the component that has a 2mm-deep pocket for wick housing. Fig. 1-bottom presents the opposite side of the same component, where the thermocouple grooves were milled. The evaporator was fabricated from a mirror-finish copperplate with dimensions 114.3 mm × 63.5 mm × 3.175 mm. On this plate, a pocket was milled with dimensions 101.6 mm × 50.8 mm × 2 mm. The remaining surrounding mirror-finish area provided the seat for the sealing gasket. A 1.59mm-diameter hole was drilled on either side of the evaporator, and a 25.4 mm long copper tube was press-fitted inside each hole. These two pipes were later used to evacuate the VC before startup and charge it with the working fluid. The copper tube was sealed on the evaporator plate with epoxy to prevent leaking. To create the wick, a 700 μm-thick copper powder was laid in the milled pocket. The sample with the copper powder was sintered at 950°C for 15 min in a single-zone tube furnace (Lindberg, Blue-M-HTF55322c) in a reducing atmosphere (90% Argon, 10% Hydrogen),with a heating ramp rate of 20 °C/min. After this process, the fused copper wick had a thickness of 500 μm and the empty vapor space of the system had a height of 3.5 mm.

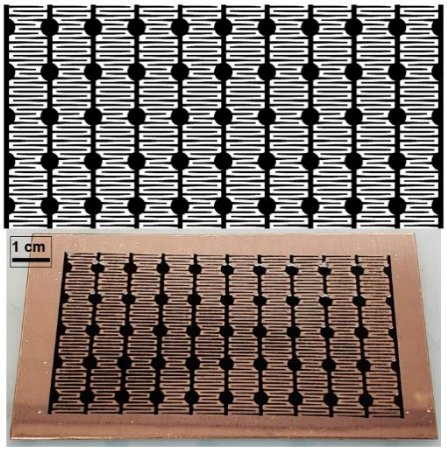

Figure 2 The wettability pattern design of the wickless condenser. At top, the pattern design is shown, while at bottom, a photograph of the condenser plate used in the experimental procedure is presented.

2) Condenser

Figure 2 shows the wettability pattern design of the wickless condenser. Fig. 2-top presents the pattern design, while Fig. 2-bottom shows a photograph of the condenser plate used in the experimental procedure. The condenser was fabricated from a mirror-finish copper plate with dimensions 114.3 mm × 63.5 × 1 mm. The surface was functionalized by spin-coating Teflon AF (AF 2400, Amorphous Fluoroplastics Solution, Chemours Co.). The sample was then cured in the same furnace in three stages, namely 80, 180 and 260°C. Next, a laser marking system (EMS400, TYKMAElectrox®, 40% power, 20 kHz intensity, 200 mm/s traverse speed) was used to etch the desired surface pattern. The laser selectively ablated the Teflon coating from the copper plate, rendering the treated domains superhydrophilic. The laser-etched sample was then immersed in an aqueous solution of 2.5 mol/L sodium hydroxide (Sigma-Aldrich, 415413-500ML) and 0.1 mol/L ammonium persulfate (Sigma-Aldrich, $\geqslant$ 98%, MKCF3704) at room temperature for 5 minutes. After this process, the laser-etched regions were covered with nanostructures [14], while the Teflon-coated mirror-finish areas remained unaltered. This process produced a wickless copper plate with a hydrophobic background and a superhydrophilic pattern.

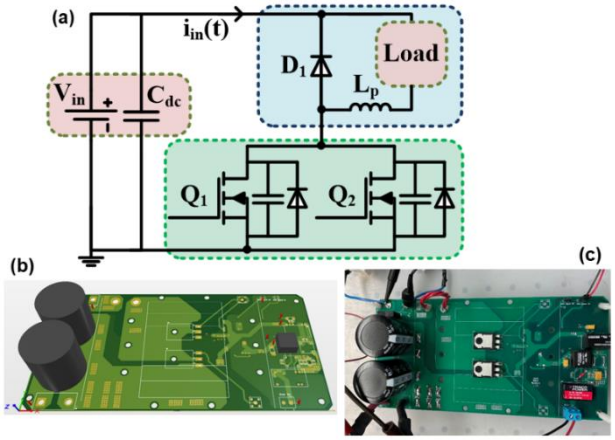

Figure 3 (a) Circuit schematic of the topology used for heat generation. (b) Experimental setup of the heat generation circuit as drawn with 3D Altium Designer. (c) Photograph of the printed circuit board.

B. Experimental Setup

1) PE Setup

Figure 3(a) presents a schematic of the topology used for heat generation, while the experimental implementation is shown in Fig. 3(b) and 3(c). The topology consists of two Si-based N-channel MOSFETs (Q_1 and Q_2) with overall 3.86 cm^2 heat dissipation area, one diode (D_1), a purely resistive load, a DC-link capacitor, and DC input. MOSFETs Q_1 and Q_2 are of the TO-247-3 package and intentionally chosen with typically 5 Ω conduction resistance for heat generation purposes. Q_1 and Q_2 are connected in parallel and can be turned on and off separately by different gate signals. The resistive load is in parallel with D_1 and then, the whole branch is in series with Q_1 and Q_2. The DC power supply, designated as V_{in}, launches energy delivery to the load whenever any of Q_1 and Q_2 is turned on. The energy transfer halts when both Q_1 and Q_2 are turned off and the current, flowing past the parasitic inductor (L_p), freewheels via D_1 under this circumstance. By doing so, Q_1 and Q_2 are turned off in a fast manner and the voltage stress across Q_1 and Q_2 is significantly reduced. The power loss of $Q_{1\text{-}2}$ (e.g., turn-on loss, conduction loss, and turn-off loss), originating from periodic switching events, dissipates through the device packaging and heats Q_1 and Q_2 up. Therefore, Q_1 and Q_2 act as heat sources for the considered VC-based cooling method.

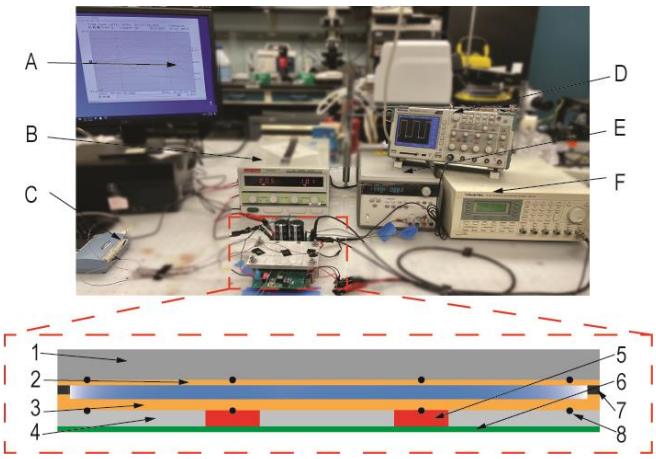

Figure 4 Photograph of the complete experimental setup (top) and schematic cross section of the vapor chamber (magnified detail at bottom) used in this work. The letter components in the photograph mark the equipment used to perform the experiments. The numeric components in the blow-up side view at bottom present the VC components that are not visible in the photograph.

2) Experiment Rig

Figure 4 presents the components of the experimental setup. To achieve adequate sealing and efficient thermal contact between the MOSFETs and the VC, all components were held between an aluminum (Al) plate [Fig. 4(1)], which acts as a heat sink, and the bench table, secured by four parallel cylindrical posts. On the top side of the VC, the wickless condenser [Fig. 4(2)] was in contact with the Al plate, while at the bottom, the wick-lined evaporator [Fig. 4(3)] was in contact with a thin Teflon piece [Fig. 4(4)] that housed the two MOSFETs [Fig. 4(5)]. The bottom side of the Teflon plate was in contact with the printed circuit board (PCB) [Fig. 4(6)]. The purpose of this arrangement was to facilitate heat flow from the MOSFETs to the VC in the most uniform way, insulating the MOSFETs sides and at the same time offering sufficient contact between the components. The evaporator

and condenser components were held apart by a 2 mm-thick gasket [Fig. 4(7)], which allowed the system to be effectively sealed while also allowing heat to be transferred from one side (evaporator) of the VC to the other (condenser). This occurred only via phase change, because there was no physical contact between the cold and hot sides of the system, resulting in negligible heat transfer by conduction. To obtain accurate temperature readings of the system's exterior, eight thermocouples (Omega, T-type, bead diameter 0.05 mm) [Fig. 4(8)] were mounted around the system's shell, four on the evaporator side and four on the condenser. Temperature was tracked in real-time [Fig. 4(A)] and captured using a data acquisition device [Fig. 4(C)] (Omega DAQ, USB 2400 series) at 1 Hz sampling frequency. To precisely control and operate the PCB, the following equipment was used: DC power supply HY10010EX [Fig. 4(B)] (output from 10 to 60 V) to control the voltage and therefore the heat input to the VC; logic power supply Agilent E3646A [Fig. 4(E)] set at 20 V to operate the PCB; waveform generator (set at 100 kHz) Wavetek Model 395 [Fig. 4(F)] to control the switching frequency of the MOSFETs; and Tektronix TPS2024B digital oscilloscope [Fig. 4(D)] to monitor the electrical signals. More equipment -not shown in Figure 4- utilized in the experiments included: A vacuum pump (Alcatel Annecy 2008A) used to rid the VC of air and non-condensable gases and set the pressure within the system at ~6.5 kPa. This pump was connected to the VC via a copper tube on the evaporator side and leak-proof tubing, with an on-off valve and a flow-adjusting valve connected in series. The on-off valve was located closest to the VC, and a vacuum gauge was installed between the two valves to measure pressure during the evacuation stage. Another copper tube was attached to the opposite side of the VC with a syringe containing pre-boiled DI water in a predefined quantity that would charge the VC with the working medium after the initial evacuation. Finally, a 12 cm × 12 cm electrical fan (Sunon, SP101A, 115 V, 0.21 A) with five blades was employed during the experiments to remove heat form the whole system. All trials were conducted under forced convection.

C. Experimental Procedure

The chamber was first sealed, and a first vacuum was drawn. As part of the initialization process, the wick was soaked with the predetermined amount of water. For 20 minutes, the VC was heated to 40°C. Following that step, a second degassing run was carried out. The system was let to re-equilibrate at room temperature, before the startup operation was completed. Two repeated trials were done under each heating condition to produce error estimates. Six different heat inputs were tested in each run, which lasted for five minutes. For the thermal evaluation of the system, the final 60 seconds of temperature data from each run were used. To protect damage to the MOSFETs, The maximum temperature of 100 ºC was chosen as the stoppage point.

D. Performance Metrics and Data Reduction

The following performance metrics were utilized to describe the system's thermal performance:

1) Thermal resistance

Thermal resistance is used to assess the VC's ability to transfer heat and should ideally be close to zero. The temperatures measured are used to compute the overall thermal resistance of the system, R_{tot} (K/W) as follows,

$$R_{tot} = \frac{\Delta T}{Q} = \frac{T_{evap}^{avg,M} - T_{cond}^{avg}}{Q_{in}} \quad (1)$$

where $T_{evap}^{avg,M}$ is the average temperature measured between the two MOSFETs and the system's evaporator side, T_{cold}^{avg} is the average temperature on the condenser side of the system measured by four thermocouples, and Q_{in} is the imposed heat load equal with the heat losses from the two MOSFETs.

2) Operating Temperatures

The temperature difference between the highest evaporator temperature and the corresponding maximum condenser temperature, measured in K, reflects the hot-spot reduction (HSR). The lower this quantity, the more efficient the system. HSR was calculated as follows:

$$HSR = T_{evap}^{max} - T_{cond}^{max} \quad (2)$$

A Gaussian error propagation analysis was performed for each of the metrics to identify the experimental errors, similar to our earlier work [9-13].

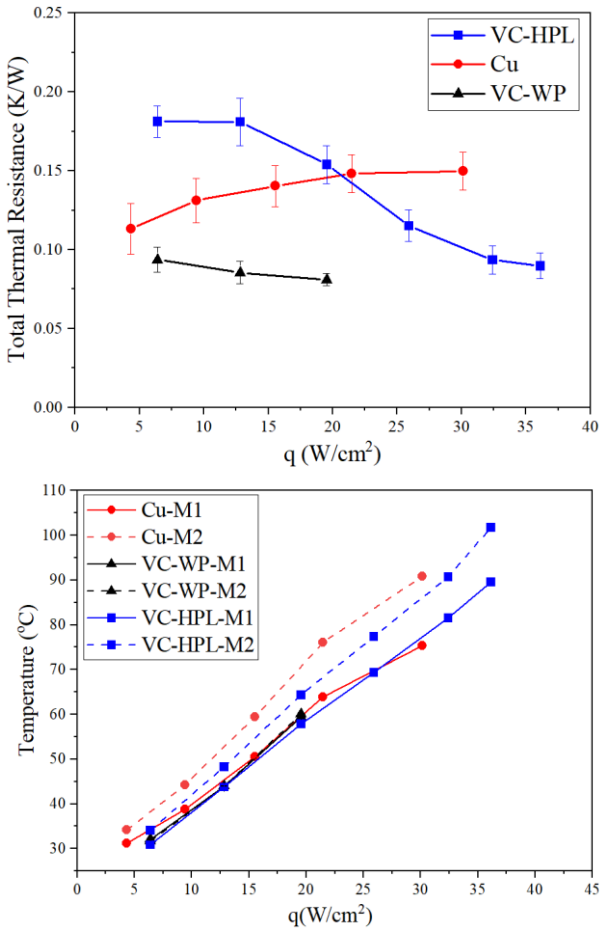

Figure 5. MOSFET total thermal resistance (top) and temperature (bottom) vs. heat flux for a plain Cu plate and the hybrid VC.

III. RESULTS AND DISCUSSION

For benchmarking purposes, a Cu plate with the same dimensions as the hybrid VC was tested under the same heat

loads. Figure 5 represents the total thermal resistance (R_{tot}) and MOSFET average temperature ($T_{evap}^{avg,M}$) vs. heat load for the Cu plate and the hybrid VC of identical dimensions with a wickless wettability-patterned (VC-WP) and uniform hydrophilic (VC-HPL) condenser. Testing of the former VC was performed only up to 20 W/cm^2, and the tests are ongoing. As shown, at lower heat fluxes a plain copper plate heat sink shows a better performance, however, as the heat flux increases, the phase change mechanism in the VC-HPL outperforms pure conduction. The lowest resistance for the Cu plate was 0.11±0.06 K/W at 4.32 W/cm^2 (16W), while the lowest values for the VC-HPL and VC-WP was 0.089±0.01 K/W at 36.12 W/cm^2 (138.72 W) and 0.081±0.005 at 20 W/cm^2 (75 W), respectively. It is important to notice that this value of R_{tot} is the lowest resistance achieved to date by a thermal-management system with a wickless and wettability patterned component. Moreover, the slopes of these lines are distinct. As heat load rises, the Cu plate curve shows a positive slope, while the VC curves show a negative slope (a desired trait). This is a favorable situation for the VC, because it shows that this system has not reached its full potential yet and it would be preferable for higher heat inputs. Furthermore, the hybrid VC is a system currently under development and it may achieve even better performance after more rigorous development, i.e. optimizing the charging ratio or vapor core thickness. At the bottom frame of Fig. 5, the temperatures of the each MOSFET (denoted by M1 and M2) are presented vs. heat input. Although the MOSFETs are provided by the same manufacturer, due to the setup design and manufacturing differences there is always a performance difference between two MOSFETs. This difference is observed for all cases with an evident temperature difference at the same heat load. Moreover, the amount of heat generated by a MOFSET is a function of its temperature so that by increasing its temperature, the performance decreases and less power could be generated with the same input voltage. As a result, the copper plate heat sink with the same input voltage could extract less power and as seen in the bottom of Fig. 5, the VCs with similar temperatures to Cu plate were able to extract larger heat load. The hot side of the Cu plate reached to 95 ^{o}C at 30.12 W/cm^2 (116.3 W), while the VC-HPL reached 104 ^{o}C at 36.12 W/cm^2 (138.72 W). Furthermore, the temperature differences between two MOSFETs are another indicator of the efficiency of the heat sink performance. As seen in Fig. 5, M1 and M2 temperature differences for the Cu plate are largest at each heat load, showing weak heat dissipation capability only by conduction heat transfer. The VC-HPL shows a lower temperature difference between M1 and M2, indicating higher efficiency compared to pure copper plate. However for a vapor chamber, it is desirable to have a high dissipation capability, rendering minimum temperature difference between M1 and M2, but the VC-HPL due to having a hydrophilic condenser could not provide a uniform dissipation since due to non-uniform condensation and random pooling on the condenser the condensation rate and condensate return path to the wick-lined evaporator is not consistent, due to hydrophilicity of the condenser plate. On the other hand, VC-WP shows minimum temperature difference between M1 and M2, reflecting a uniform heat dissipation due to a controlled condensation on the condenser and an organized and continuous return of the condensate to the wick-lined evaporator, as reported in our previous works [9-12]. This resulted in the lowest average temperature of the MOSFETs with minimal temperature differences among all cases up to 20 W/cm^2 heating load.

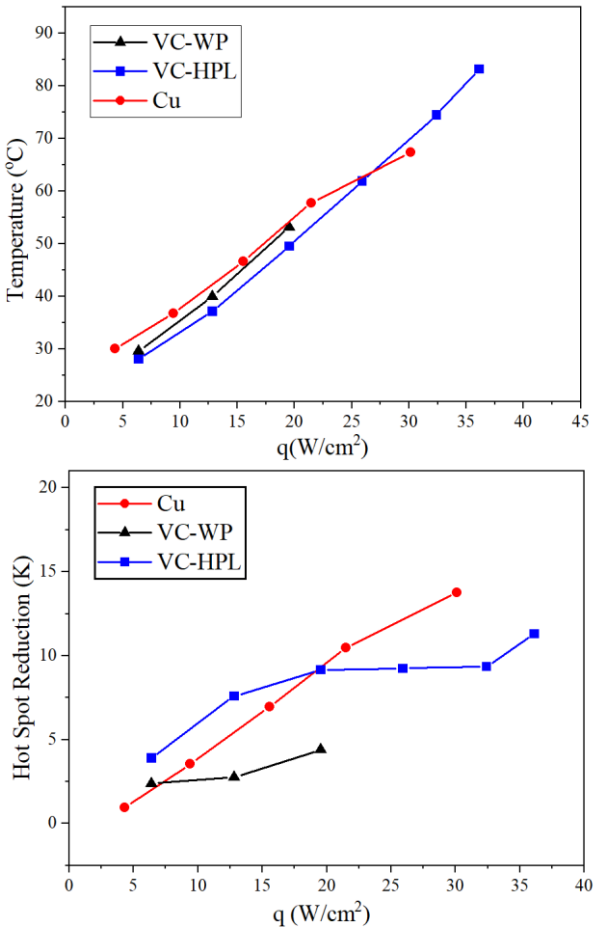

Figure 6.Cooled side (Condenser) temperature and hot-spot temperature reduction vs. heat flux for a plain Cu plate and the hybrid VC.

Figure. 6 presents the average cooled side (condenser for VCs) temperatures and the hot-spot temperature reduction (*HSR*) from the evaporator to the condenser vs. heat input for all cases. As seen, the cooled side temperatures of the copper plate is higher than that of the VCs at low heat fluxes as the conduction prevails. However, the VC-WP shows higher temperature compared to WP-HPL due to high condensation heat transfer of wettability-patterned surfaces [15].

At the bottom frame of Fig. 6, the hot-spot temperature reduction from the evaporator to the condenser is presented vs. heat input. As expected, the HSR of copper plate is progressively increasing, indicating larger temperature difference between the heat sources and the cooled side of the heat sink and inefficiency of conduction heat transfer at high heat fluxes. On the other hand, the VC-HPL shows an initial increase of HSR followed by a steady trend till 32.4 W/cm^2, where an increase is observed, hinting to a partial dryout at the heating area. The VC-WP shows the lowest HSR, pointing to minimum temperature difference between the evaporation and condensation areas due to a uniform and controlled condensation mechanism and a constant and uninterrupted resupply of the wick structure thanks to the wettability pattern.

IV. CONCLUSION

This work described a hybrid vapor chamber-based system, comprised of a wick-lined evaporator and a wickless wettability-patterned condenser, to thermally control and cool down a custom power electronics system. This VC prototype is based on our previous work on wickless and wettability-patterned thermal management systems whose operation relies on phase change. The VC was redesigned, built and investigated experimentally in the area of power electronics and its performance was compared against a Cu slab heat sink with the same dimensions. The main attribute of this apparatus is that it is the first hybrid system of its kind with a rectangular and not fully symmetrical shape. At the same time, the system has the ability to accommodate multiple (two in the present case) distinct heat sources. Moreover, this system had competitive heat transfer characteristics with thermal resistance as low as 0.081±0.005 K/W at 75 W. This system demonstrates the scalability and adaptability of our already presented technique [9-13] of wettability-pattern utilization in thermal-management systems. Finally, a novel experimental setup was demonstrated, which was comprised of a PCB populated by two MOSFETs of TO-247-3 packaging, connected in parallel to achieve higher current capability, and switched at 100 kHz. This setup was fabricated to emulate high-power applications on a low-power experimental setup of reduced cost, and represents modern power electronics applications; therefore, it can be scaled to other power electronic systems requiring advanced cooling. The reported VC performance can be further improved by fine-tuning the amount of working liquid (charging load) and the wettability pattern, but this is left for follow-up studies in the future.

ACKNOWLEDGMENT

This material is based upon research supported by, or in part by, the U. S. Office of Naval Research under award number N00014-20-1-2025 to the University of Nebraska, Lincoln and a subaward to the University of Illinois at Chicago. The authors thank J. Rodriguez (Assistant Director) and T. Bruzan (Laboratory Mechanic) at the UIC College of Engineering Scientific Instrument/Machine Shop for machining the samples.

REFERENCES

[1] Shrestha, N. M., Li, Y., Chen, C. H., Sanyal, I., Tarng, J. H., Chyi, J. I., & Samukawa, S. (2020). Design and Simulation of High Performance Lattice Matched Double Barrier Normally Off AlInGaN/GaN HEMTs. IEEE Journal of the Electron Devices Society, 8, 873-878.

[2] Bao, C., & Mazumder, S. K. (2021, June). GaN-HEMT based very-high-frequency ac power supply for electrosurgery. In 2021 IEEE Applied Power Electronics Conference and Exposition (APEC) (pp. 220-225). IEEE.

[3] Chatterjee, D., & Mazumder, S. K. (2021). Switching Transition Control to Improve Efficiency of a DC/DC Power Electronic System. IEEE Access, 9, 91104-91118.

[4] Kumar, N., Mohamadi, M., & Mazumder, S. K. (2020). Passive Damping Optimization of the Integrated-Magnetics-Based Differential-Mode Ćuk Rectifier. IEEE Transactions on Power Electronics, 35(10), 10008-10012.

[5] Lu, T. J. (2000). Thermal management of high power electronics with phase change cooling. International journal of heat and mass transfer, 43(13), 2245-2256.

[6] Ju, Y. S., Kaviany, M., Nam, Y., Sharratt, S., Hwang, G. S., Catton, I., Dussinger, P. (2013). Planar vapor chamber with hybrid evaporator wicks for the thermal management of high-heat-flux and high-power optoelectronic devices. International Journal of Heat and Mass Transfer, 60, 163-169.

[7] Chen, Y., Li, B., Wang, X., Wang, X., Yan, Y., Li, X., ... & Li, H. (2020). Direct Phase-Change Cooling of Vapor Chamber Integrated With IGBT Power Electronic Module for Automotive Application. IEEE Transactions on Power Electronics, 36(5), 5736-5747.

[8] Yi, L., Hu, H., Zhang, Y., Yang, S., & Pan, M. (2021). Experimental investigation on enhanced flow and heat transfer performance of micro-jet impingement vapor chamber for high power electronics. International Journal of Thermal Sciences, 107380.

[9] Koukoravas, T. P., Damoulakis, G., & Megaridis, C. M. (2020). Experimental investigation of a vapor chamber featuring wettability-patterned surfaces. Applied Thermal Engineering, 178, 115522.

[10] Damoulakis, G., Jafari-Gukeh, M., Koukoravas, T. P., & Megaridis, C. (2021). High-performance Planar Thermal Diode with Wickless Components. Journal of Electronic Packaging.

[11] Gukeh, M. J., Damoulakis, G., & Megaridis, C. M. (2021, June). Experimental investigation of low-profile heat pipe with wickless wettability-patterned condenser. In 2021 20th IEEE Intersociety Conference on Thermal and Thermomechanical Phenomena in Electronic Systems (iTherm) (pp. 271-279). IEEE.

[12] Damoulakis, G. and Megaridis, C. M. (2021), Wick-Free Paradigm for High-Performance Vapor-Chamber Heat Spreaders. Energy Conversation and. Management, in press.

[13] Damoulakis, G., Kaufman, G., Tsubaki, A., Gogos, G., Zuhlke, C., & Megaridis, C. M. (2021, June). Vapor Chamber Thermal Diode with Laser-fabricated Wickless Components. In 2021 20th IEEE Intersociety Conference on Thermal and Thermomechanical Phenomena in Electronic Systems (iTherm) (pp. 246-253). IEEE.

[14] Zhang, W., Wen, X., Yang, S., Berta, Y., & Wang, Z. L. (2003). Single‐crystalline scroll‐type nanotube arrays of copper hydroxide synthesized at room temperature. Advanced materials, 15(10), 822-825.

[15] Ghosh, A., Beaini, S., Zhang B. J., Ganguly, R., and Megaridis, C. M. "Enhancing dropwise condensation through bioinspired wettability patterning." *Langmuir* 30, no. 43 (2014): 13103-13115.